Orientation of Tryptophan-26 in Coat Protein Subunits of the Filamentous Virus *Ff* by Polarized Raman Microspectroscopy†

Masamichi Tsuboi,‡ Stacy A. Overman, and George J. Thomas, Jr.*

Division of Cell Biology and Biophysics, School of Biological Sciences, University of Missouri−Kansas City, Kansas City, Missouri 64110

Received November 22, 1995; Revised Manuscript Received June 10, 1996⊗

ABSTRACT: The *Ff* filamentous virus, which includes the closely related strains *fd*, *f1*, and *M13*, serves as a model for membrane protein assembly and is employed extensively as a cloning vector and vehicle for peptide display. The threadlike virion (≈6 × 880 nm) comprises a single-stranded DNA genome sheathed by ≈2700 copies of a 50-residue α-helical subunit, the product of viral gene VIII. The pVIII subunit contains a single tryptophan residue (tryptophan-26) which is essential for assembly. We have employed polarized Raman microspectroscopy to determine the orientation of tryptophan-26 in pVIII subunits of oriented *fd* fibers. The present application is based upon the transfer of tryptophan Raman tensors from a recent study of *N*-acetyl-L-tryptophan single crystals [Tsuboi *et al*. (1996) *J. Mol. Struct. 379*, 43−50]. The polarized Raman spectra of *fd* indicate that the plane of the indole ring in each pVIII subunit is close to parallel to the virion axis. In this orientation, the line connecting indole ring atoms N1 and C2 is nearly perpendicular to the virion axis, while the indole pseudo-2-fold axis (a line connecting atom C2 to the midpoint of the C5−C6 bond) is approximately 36° from the virion axis. We have used the present results in combination with preferred tryptophan side-chain torsions [χ^1 (C3−Cβ−Cα−N) and $\chi^{2,1}$ (C2−C3−Cβ−Cα)] in other proteins and a previously determined experimental value of $\chi^{2,1}$ in *fd* [Aubrey, K. L., & Thomas, G. J., Jr. (1991) *Biophys. J. 60*, 1337−1349] to propose a detailed molecular model for the orientation of the tryptophan-26 side chain in the native virus.

Ff is the class prototype of long (≈880 nm) and thin (≈6 nm diameter) bacterial viruses infecting F^+ strains of *Escherichia coli*. Phages *fd*, *f1*, and *M13* are morphologically identical members of the *Ff* class, in which a single-stranded DNA loop of 6410 nucleotides is packaged within a sheath comprising about 2700 copies of a 50-residue subunit (pVIII), the product of viral gene VIII. *Ff* is an important tool in experimental molecular biology, serving as a cloning vector (Denhardt *et al.*, 1978), a substrate for antigenic peptide display (Smith, 1985; Scott & Smith, 1990; Greenwood *et al.*, 1991), a vehicle for sequence specific DNA recognition (Choo & Klug, 1994; Jamieson *et al.*, 1994), and a model for nucleoprotein assembly within a membrane bilayer (Russel, 1994). Although many genetically engineered mutants of *Ff* virions have been described, in no case has the mutation of tryptophan-26 (W26) yielded a viable phage product (Williams *et al.*, 1995). The widespread use of *Ff* has prompted numerous investigations of the virion architecture, including structural studies by fiber X-ray diffraction (Marvin *et al.*, 1974, 1994; Makowski & Caspar, 1981; Marvin, 1990; Glucksman *et al.*, 1992), solid state NMR spectroscopy (Cross *et al.*, 1983; Opella *et al.*, 1987; Opella & McDonnell, 1993), solution Raman spectroscopy (Thomas & Murphy, 1975; Thomas *et al.*, 1983; Overman & Thomas, 1995), and solution CD spectroscopy (Clack & Gray, 1989, 1992; Arnold *et al.*, 1992). A review is given in Day *et al.* (1988). The results show that pVIII subunits are uniformly α-helical and layered about the filament axis with 5-fold rotational symmetry and an approximately 2-fold screw axis. A high-resolution structural model of the virion is, however, not available.

Recently, polarized Raman spectroscopy was applied to *fd* to determine that the average angle of inclination (tilt) of the pVIII α-helix with respect to the filament axis is 16 ± 4° (Overman *et al.*, 1996). Model-building studies based upon X-ray and NMR results (Marvin *et al.*, 1974, 1994; Marvin, 1990; Makowski & Caspar, 1981; Cross *et al.*, 1983; Opella *et al.*, 1987; Marzec & Day, 1988; Glucksman *et al.*, 1992; Opella & McDonnell, 1993) have suggested a helix tilt angle between 0 and 30°, in reasonable accord with the experimental value. Nevertheless, the orientations and interactions of subunit side chains in the virion assembly remain largely unknown, and additional experimental data are required to determine them. Knowledge of the pVIII side chain conformations and environments should enable more accurate modeling of protein-protein and protein−DNA interfaces within the virion. Detailed structural information on the pVIII side chains should also advance understanding of filamentous phage polymorphism (Hemminga *et al.*, 1992) and its relevance to proposed assembly and disassembly mechanisms.

Here we employ polarized Raman microspectroscopy to determine the orientation of the unique tryptophan side chain (W26) of pVIII in the native *fd* assembly. The present application involves measurement of polarized Raman spectra from uniformly oriented fibers of *fd* filaments by use of a Raman microscope. The polarized Raman intensities

† Paper LII in the series Studies of Virus Structure by Raman Spectroscopy. Supported by Grant GM50776 from the U. S. National Institutes of Health.

* Author to whom correspondence should be addressed.

‡ Permanent address: Department of Fundamental Science, Iwaki-Meisei University, Iwaki, Fukushima 970, Japan.

⊗ Abstract published in *Advance ACS Abstracts,* August 1, 1996.

S0006-2960(95)02770-X CCC: $12.00

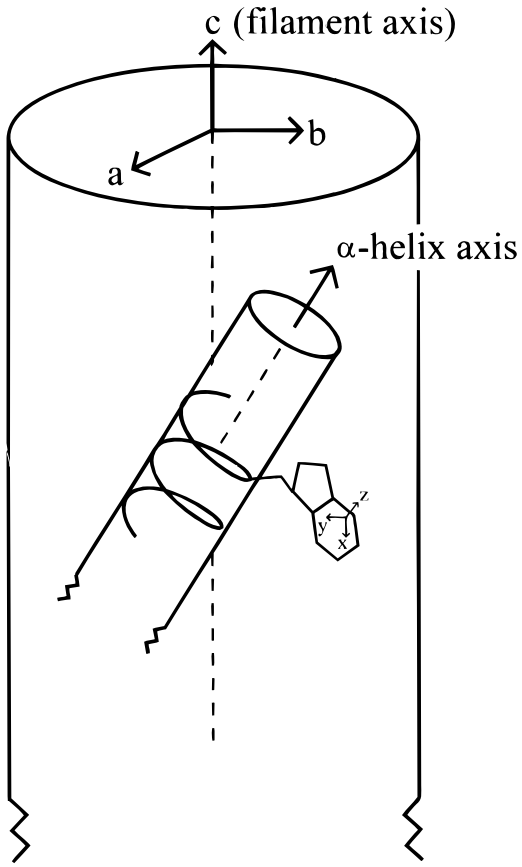

FIGURE 1: Coordinate system (*a*, *b*, *c*) for a uniaxially oriented fiber of the *fd* virus and the set of principal axes (*x*, *y*, *z*) corresponding to a representative Raman tensor of the indole ring of tryptophan-26. The illustration is not drawn to scale, and only short segments of the 880 nm virion and 50-residue subunit are represented.

are analyzed quantitatively in terms of the tryptophan local Raman tensors. The tensors were determined in a recent polarized Raman study of a single crystal of *N*-acetyl-L-tryptophan (*N*-AcTrp) (Tsuboi *et al.*, 1996). The presently determined tryptophan orientation in the *fd* fiber is compared with the result obtained by use of an independent Raman-based method, utilizing hydrodynamic shear force to orient *fd* filaments in solution (Takeuchi *et al.*, 1996).

METHODS OF PROCEDURE

(1) Theoretical Background

In the *fd* fiber, all subunits and therefore all tryptophans are arranged uniaxially. Figure 1 illustrates schematically the two coordinate systems, (*a*, *b*, *c*) and (*x*, *y*, *z*), employed in the present analysis. The system (*a*, *b*, *c*) is fixed on the cylindrically symmetric virus particle, with *c* parallel to the virion axis and *a* and *b* equivalent and perpendicular to *c*. The coordinate system (*x*, *y*, *z*) constitutes the set of *principal axes of a single normal mode of vibration* localized in the indole ring of tryptophan-26 (W26). Because all pVIII subunits and therefore all W26 residues are arranged symmetrically with respect to the virion axis, the set of principal axes for a given normal mode is also arranged symmetrically with respect to the virion axis. Note, however, that each normal mode of W26 has a unique set of principal axes. Consequently, the principal axis system (*x*, *y*, *z*) corresponding to a given Raman band is generally different from that of every other Raman band and is uniquely situated with respect to the indole ring. The orientation of each axially symmetric and unique (*x*, *y*, *z*) system can be expressed by the two Eulerian angles, θ and χ, as illustrated in Figure 2.

We assign a Raman tensor, $\boldsymbol{\alpha}$, corresponding to each normal mode of vibration (Raman band) of the uniaxially arranged tryptophans. The Raman tensor has diagonal elements α_{xx}, α_{yy}, and α_{zz}. Physically, each tensor element is defined as a first derivative of the polarizability with respect to the vibrational normal coordinate and expresses directional change of polarizability during vibration. We deal only with the relative magnitudes of these tensor components, namely $\alpha_{xx}/\alpha_{zz} \equiv r_1$ and $\alpha_{yy}/\alpha_{zz} \equiv r_2$ (Tsuboi *et al.*, 1991; Thomas & Tsuboi, 1993). Thus, highly anisotropic Raman tensors are characterized by values of r_1 and/or r_2 which differ greatly from unity, whereas isotropic Raman tensors exhibit $r_1 \approx r_2 \approx 1$. The values of r_1 and r_2 associated with a specific vibration can be calculated from knowledge of the appropriate polarized Raman band intensities, I_{kl}, where k and l (=*a*, *b*, *c*) are the directions of incident and scattered electric vectors, respectively, in the coordinate system fixed on the fiber (Benevides *et al.*, 1993).

As noted above, the orientation of a molecular group with tensor principal axes *x*, *y*, and *z* in relation to a uniaxial lattice with axes *a*, *b*, and *c* is given by two angles, θ and χ (Figure 2). Here, θ is the angle by which *z* is tilted from the fiber axis *c*, and χ is the angle between lines O−N and O−*y* of Figure 2. Note that O−N represents the intersection between the plane of the indole ring and the plane normal to the fiber axis. The polarized Raman intensity ratio I_{cc}/I_{bb} is given in terms of θ and χ by eq 1 (Tsuboi *et al.*, 1991).

$$\frac{I_{cc}}{I_{bb}} = 4[\sin^2\theta\,(r_1\cos^2\chi + r_2\sin^2\chi) + \cos^2\theta]^2/ [\cos^2\theta\,(r_1\cos^2\chi + r_2\sin^2\chi) + (r_1\sin^2\chi + r_2\cos^2\chi) + \sin^2\theta]^2 \quad (1)$$

(2) Applications

In using eq 1 to determine the orientation of a given molecular group in the *fd* fiber, several specific cases can be noted.

Case I. Assume that for a single Raman band, the Raman tensor principal axes (*x*, *y*, *z*) and ratios (r_1, r_2) are known and the polarized Raman intensity ratio (I_{cc}/I_{bb}) is measured. In this case, the orientation of the functional group cannot be determined uniquely. Only a parametric relation between the angles θ and χ can be obtained.

Case II. If, in addition to the data of case I, it is known that $r_1 = r_2$ ($\equiv r$), i.e. the local Raman tensor is axially symmetric along *z* and $\alpha_{xx} = \alpha_{yy}$, then eq 1 becomes

$$\frac{I_{cc}}{I_{bb}} = \frac{4(r\sin^2\theta + \cos^2\theta)^2}{(r\cos^2\theta + r + \sin^2\theta)^2} \quad (2)$$

and measurement of I_{cc}/I_{bb} allows determination of the tilt angle θ. An application in which the polarization of the Raman amide I band is employed to determine the tilt angle of the subunit α-helical axis in *fd* has been described (Overman *et al.*, 1996).

Case III. If, in addition to the data of case II, it is known that $r = 1$, i.e. the local Raman tensor is isotropic, then eq

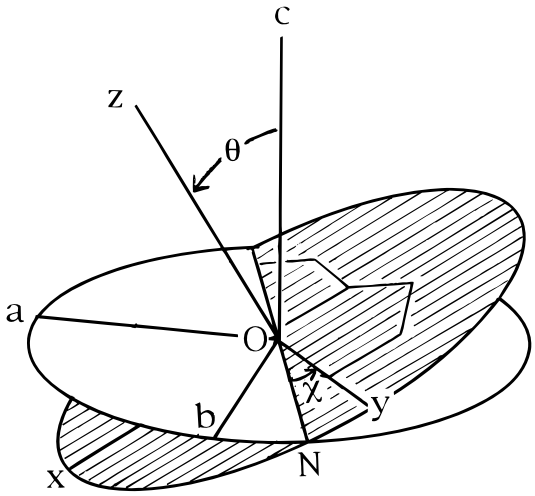

FIGURE 2: Definitions of the Eulerian angles θ and χ which designate the orientation of principal axes (x, y, z) of a tryptophan Raman tensor with respect to the *fd* fiber axes (a, b, c). Here, θ is the angle by which the Raman tensor principal axis z (perpendicular to the indole plane) is tilted from the fiber axis (c), and χ is the angle between the Raman tensor principal axis y (line O−y) and the line of intersection (O−N) between the plane of the indole ring and the plane normal to the fiber axis. An increase in χ corresponds to a counterclockwise rotation of the indole plane about the positive z axis.

2 yields $I_{cc}/I_{bb} = 1$. Accordingly, no directional information can be inferred from the data. The same result may arise for an intrinsically anisotropic local tensor if the lattice (fiber) contains a number of equivalent molecular groups in different orientations with respect to the (a, b, c) system so that the average nonlocal Raman tensor effectively gives $\alpha_{xx} = \alpha_{yy} = \alpha_{zz}$.

Case IV. In this case, the molecular group in question exhibits more than one Raman band, and for each band (i), the principal axes (x_i, y_i, z_i) and local Raman tensor components are known. Then a contour line of the polarized Raman intensity ratio [$I_{cc}(i)/I_{bb}(i)$] may be drawn in $\theta_i-\chi_i$ space for the given Raman band. The point of intersection of all such contour lines, transformed into the same $\theta-\chi$ space, yields the orientation of the molecular group. In general, the required coordinate transformation is not simple and may be intractable.

Case V. If, in addition to the data of case IV, the principal axis systems for bands i and j have a common z axis, such that a simple coordinate transformation allows the contour line in $\theta_i-\chi_i$ space to be shifted to that of $\theta_j-\chi_j$ space, then the coordinate transformation referred to above is tractable. In such a case, the orientation of the molecular group is readily determined. As shown below, this situation applies to the W26 indole ring of pVIII subunits in the *fd* fiber.

(3) Materials

Growth media and standard reagents were obtained from Sigma Chemical Co. (St. Louis, MO) and Fisher Scientific (St. Louis, MO). The *N*-AcTrp crystal which provided the Raman tensors for use in this study has been described (Tsuboi *et al.*, 1996).

The *fd* virus was grown in MS media on *E. coli* strain Hfr3300, using stocks obtained from Dr. Loren A. Day, Public Health Research Institute, New York, NY. Details of phage isolation, purification, and preparation for Raman spectroscopy have been described (Overman & Thomas, 1995).

The virus solution (≈50 mg/mL) was drawn into an oriented fiber with an ≈0.5 mm thickness by slowly drawing a spherical drop between the glass rods of a fiber-pulling device which was maintained in a hygrostatic environment (92% relative humidity). Unidirectional orientation of virions within the fiber was assessed by observing that the maximum Raman anisotropy was observed for parallel and perpendicular alignments of the fiber with respect to the electric vector of either the incident or scattered radiation. Refractive effects observed in viewing the fiber through crossed polarizers were also consistent with a high degree of orientational order in the domains of the fiber through which the laser was directed. Similar Raman polarization effects were observed for fibers drawn in a high magnetic field, for which orientational disorder is believed to be insignificant (D. A. Marvin, personal communication). The high degree of uniaxial orientation in domains of fibers probed by the laser presumably reflects the capability of selecting for optimally oriented virions with the narrow beam diameter ($<5\ \mu$m). Further consideration of the effects of imperfectly oriented virions is given in the Results and Conclusions.

(4) Raman Microspectroscopy

The instrumentation for polarized Raman microscopy combines a Coherent INNOVA 70 argon laser (Santa Clara, CA), an Olympus model BHSM microscope (Lake Success, NY), an ISA/Jobin-Yvon model S3000 triple spectrograph (Edison, NJ), and an ISA Spectraview-2D charge-coupled-device detector and has been described in detail (Benevides *et al.*, 1993; Thomas *et al.*, 1995).

The experimental arrangement employs a narrowly focused laser beam (diameter ≈1 μm), which permits data collection from highly crystalline domains within the fiber of uniaxially oriented viral filaments. The fiber was maintained at a constant relative humidity of 92% and thermostatted at 10 °C throughout the data collection protocols.

RESULTS AND CONCLUSIONS

Polarized Raman spectra in the 300−1800 cm^{-1} region for *cc* (I_{cc}) and *bb* (I_{bb}) orientations of the *fd* virus are shown in Figure 3. In Figure 4, the segments of the spectra containing the most important tryptophan marker bands are redrawn on an expanded scale. Figure 4 also illustrates the principal axes (x, y, z) and respective Raman tensor ratios (r_1, r_2) for the 1340, 1364, and 1560 cm^{-1} bands of the W26 residue in *fd*.

The Raman tensors employed in Figure 4 were determined from a polarized Raman study of an oriented single crystal of *N*-AcTrp (Tsuboi *et al.*, 1996). It is assumed that these tensors can be transferred without change to the W26 residue of pVIII in the *fd* assembly (see Summary and Discussion). The tryptophan Raman frequencies and polarized Raman intensities from spectra of Figures 3 and 4 and the corresponding Raman tensors transferred from *N*-AcTrp are summarized in Table 1. More detailed tabulations of aromatic side-chain assignments in *fd* are given elsewhere (Aubrey & Thomas, 1991; Overman & Thomas, 1995).

The W26 residue makes major contributions to the *fd* spectrum at 758, 879, 1010, 1340, 1364, 1560, and 1582 cm^{-1}. For all but the band at 879 cm^{-1}, the Raman tensors

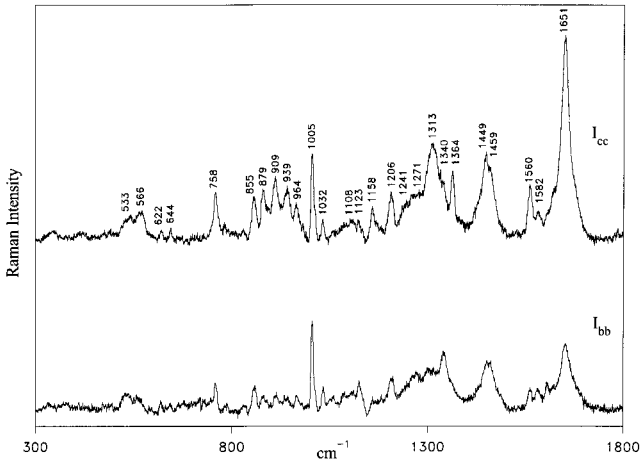

FIGURE 3: Polarized Raman spectra in the 300−1800 cm^{-1} region for *cc* (I_{cc}) and *bb* (I_{bb}) orientations of the *fd* virus excited at 514.5 nm. Relative intensities, which were collected in immediate succession on the same fiber after rotation by 90° on the microscope platform, are believed to be accurate to within 2%. Further details of the apparatus and experimental protocol have been given by Benevides *et al.* (1993).

are known (Tsuboi *et al.*, 1996). Of these, the bands at 758 and 1010 cm^{-1} are characterized by essentially isotropic tensors (case III, above), and therefore, their polarized Raman intensity ratios are not of value for assessing tryptophan residue orientation. This is apparent for the band at 1010 cm^{-1} in Figure 3, occurring in both I_{cc} and I_{bb} spectra as a weak shoulder to the more prominent band of phenylalanine at 1005 cm^{-1}. Note that, in the case of *fd*, the isotropic band at 758 cm^{-1} and also the band at 1582 cm^{-1} are complicated by overlap from bands of either DNA, the peptide backbone, or various side chains (Overman & Thomas, 1995; S. A. Overman and G. J. Thomas, Jr., unpublished results). Consequently, the polarizations observed in Figure 3 for the *fd* bands at 758 and 1582 cm^{-1} are not governed solely by the orientation of W26.

The Raman tensors for the 1364 and 1560 cm^{-1} modes are highly anisotropic, and the corresponding bands in the *fd* spectrum are sharp and their intensities accurately measurable. For the 1560 cm^{-1} vibration, the greatest polarizability change is along the line (pseudo-2-fold axis) intersecting C2 and bisecting the C5−C6 bond. This conclusion is based upon the fact that the indole pseudo-2-fold axis in the *N*-AcTrp single crystal coincides with the crystallographic *b* axis, and the finding that only the I_{bb} component of the polarized Raman spectrum exhibits an intense 1560 cm^{-1} band (Tsuboi *et al.*, 1996). Because of the high value of the polarized Raman intensity ratio of *fd* at 1560 cm^{-1} ($I_{cc}/I_{bb} = 2.8 \pm 0.2$), it is clear that the pseudo-2-fold axis of W26 is oriented more or less along the *fd* fiber axis (*c*). A more quantitative assessment is obtained as follows.

The specific orientation of the indole ring in *fd* can be determined by application of eq 1 to Raman bands of the W26 residue at 1364 and 1560 cm^{-1}. For the band at 1560 cm^{-1}, substitution of the experimental values of $I_{cc}/I_{bb} = 2.8 \pm 0.2$, $r_1 = 0.59$, and $r_2 = 2.71$ (Figure 4 and Table 1) into eq 1 yields the set of (θ, χ) values represented by the horizontally hatched area of Figure 5A. Any (θ, χ) pair within this region is consistent with the experimental data (case I above). Similarly, the region of (θ, χ) space allowed by the polarization of the 1364 cm^{-1} band is indicated in Figure 5A by vertical hatch marks.

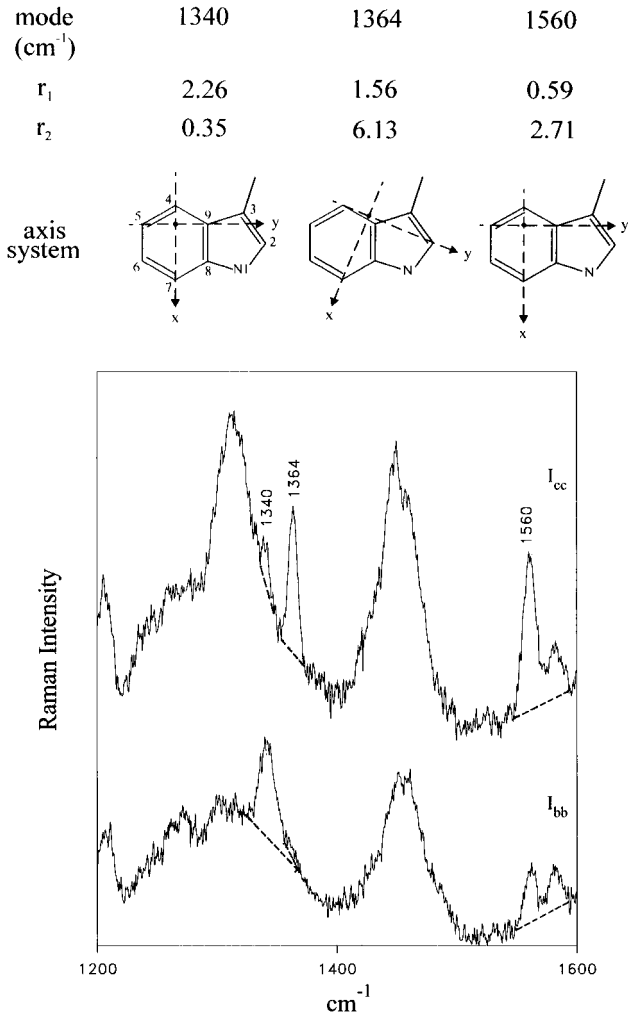

FIGURE 4: The rectangular box contains expanded scale presentations of the polarized Raman spectra of *fd* in the 1200−1600 cm^{-1} region (I_{cc}, upper trace; I_{bb}, lower trace). Labels indicate the important tryptophan markers at 1340, 1364, and 1560 cm^{-1}, which are discussed in the text. Dashed lines indicate the baselines over which the polarized Raman intensities have been measured. Above the box are illustrated the sets of principal axes (*x*, *y*, *z*, with only *x* and *y* labeled) and Raman tensors (r_1 and r_2) corresponding to each tryptophan marker.

Table 1: Raman Tensors and Polarizations for Bands of Tryptophan-26 in the Spectrum of the *fd* Virus

Raman band (cm^{-1})	Raman tensor[a] r_1	r_2	polarization, I_{cc}/I_{bb}
758	1.78	0.83	*b*
1010	1.74	0.87	≈1
1340	2.26	0.35	0.4 ± 0.2
1364	1.56	6.13	20 ± 5
1560	0.59	2.71	2.8 ± 0.2
1582	−0.7	6.1	*b*

[a] From Tsuboi *et al.* (1996). [b] Not determined due to overlap with Raman bands of other viral components. See the text.

Note from Figure 4 that the 1364 cm^{-1} tensor is defined using a set of principal axes (Trp2) differing from the set (Trp1) employed for the 1560 cm^{-1} band. As shown previously (Tsuboi *et al.*, 1996), this difference is equivalent to a 22° rotation in χ about the *z* axis common to Trp1 and Trp2. Consequently, in order to locate the region of (θ, χ) space in Figure 5A compatible with both the 1560 and 1364 cm^{-1} Raman bands, it is necessary to reduce the angle χ of

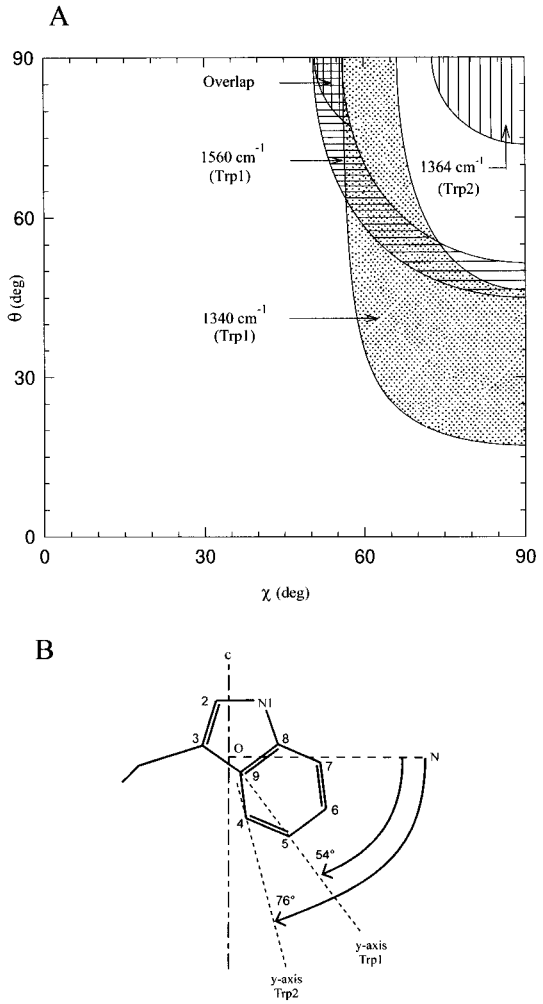

FIGURE 5: (A) Maps of I_{cc}/I_{bb} in (θ, χ) space for the tryptophan-26 Raman bands of *fd* at 1340 (stippling), 1364 (vertical hatching), and 1560 cm^{-1} (horizontal hatching). Shaded areas indicate (θ, χ) domains consistent with experimentally observed values of I_{cc}/I_{bb}, assuming Raman tensors and principal axes (Figure 4) transferred from *N*-AcTrp (Tsuboi *et al.*, 1996). The area of overlap of stippling with vertical and horizontal hatching, which is labeled at the top of the map, indicates the (θ, χ) values in the Trp1 coordinate system which identify the orientation of the indole ring of tryptophan-26 in the *fd* subunit. See the text. (B) Illustration of the indole ring orientation of tryptophan-26 as determined in panel A. The *c* axis and the O−N line are defined in Figure 2.

Trp2 by 22°. This transformation corresponds to case V (above) and is represented in Figure 5A by the area containing the overlap of horizontal and vertical hatching, accomplished by translating the latter along the $\theta = 90°$ line so that it eclipses the former as shown in the figure.

In Figure 5A, we also show the area of (θ, χ) space which corresponds to experimental data for the 1340 cm^{-1} band. The large area of this region (stippled) reflects the fact that measurement of the 1340 cm^{-1} band intensity is subject to a relatively large uncertainty ($I_{cc}/I_{bb} = 0.4 \pm 0.2$), owing to the inherent weakness of the band in the I_{cc} spectrum and its severe overlap by very strong amide III bands in both I_{cc} and I_{bb} spectra. Nevertheless, as shown in Figure 5A, the polarization of the 1340 cm^{-1} band is reasonably consistent with the results for the 1364 and 1560 cm^{-1} bands. The indole orientation is thus represented in the Trp1 system by the pair ($\theta = 90°$, $\chi = 54°$) at the center of the overlapping hatched areas of Figure 5A.

The $\theta = 90°$ and $\chi = 54°$ pair fixes the indole plane as follows. Because θ is the angle between the normal to the indole plane and the virion axis, the value $\theta = 90°$ places the indole plane at 0° (i.e. *parallel*) to the virion axis. Further, the value $\chi = 54°$ places the line O−N (defined in Figure 2) at an angle of 54° from the line connecting indole atoms C5 and C9 or at an angle of 76° from the line connecting indole atoms C4 and C2, as depicted in Figure 5B. In this orientation, the indole pseudo-2-fold axis is directed at an angle of 36° from the virion axis. The latter parameter provides a convenient basis for comparison with another recent experimental determination of the W26 orientation (Takeuchi *et al.*, 1996), as noted in Summary and Discussion.

We next consider the sources of experimental error and related uncertainties in the present measurements. The most obvious source of error is due to measurement of the Raman intensities, I_{cc} and I_{bb}, in each sampling protocol. In a typical protocol, consisting of six spectral accumulations, the signal-to-noise ratios and uncertainties in the spectral baselines combine to introduce error limits of 25 and 7%, respectively, in the quotient I_{cc}/I_{bb} for bands at 1364 and 1560 cm^{-1} (Table 1). These uncertainties are reflected in the widths of the belts drawn in (θ, χ) space in Figure 5A. Thus, the range $2.6 < I_{cc}/I_{bb} < 3.0$ for the polarized Raman intensity ratio of the 1560 cm^{-1} band corresponds to ranges in the Eulerian angles of $51° < \chi < 57°$ at constant θ (=90°) and of $78° < \theta < 102°$ at constant χ (=54°). Similarly, the range $15 < I_{cc}/I_{bb} < 25$ for the polarized Raman intensity ratio of the 1364 cm^{-1} band corresponds to $73° < \chi < 90°$ at constant θ (=90°), and $80° < \theta < 100°$ at constant χ (=76°). Combining the data for the 1364 and 1560 cm^{-1} bands, using the Trp2 → Trp1 axis transformation outlined above, restricts the range of uncertainty to points within the overlapping belts. Accordingly, a reasonable estimate of the uncertainty in the (θ, χ) pair is (90 ± 10°, 54 ± 3°).

A second potential source of error can be attributed to imperfect orientation of the filamentous virions within the fiber. A detailed consideration of this effect has been given previously (Overman *et al.*, 1996). In short, this effect can be estimated by assuming a Gaussian disorder distribution with a half-width 2*d* and allowing for tilt of the fiber by an angle δ along any meridian from the fiber axis so that the number of tilted virions is proportional to $(\sin \delta)[f(\delta)]$, where $f(\delta) = \exp(-0.693\delta^2/d^2)$. The Raman intensities are then calculated after substitution of tensor ratios appropriately weighted with $(\sin \delta)[f(\delta)]$ and integrated over the interval $0 < \delta < \pi/2$. The dependence of I_{cc}/I_{bb} on the disorder parameter *d* has been calculated for several possible angles of inclination of the pVIII helix from the filament axis. The I_{cc}/I_{bb} ratio of 3.0 for the amide I band at 1650 cm^{-1} was found to be consistent with a helix tilt of 16° and small misalignment ($0 < d < 3°$) or tilt of 13° and more substantial misalignment ($d \approx 9°$). Helix tilt angles greater than 20° are not consistent with the polarized Raman amide I data (Overman *et al.*, 1996). Because the *fd* fiber samples generating the data of Figures 3 and 4 exhibit the same I_{cc}/I_{bb} ratio (3.0 ± 0.2) observed by Overman *et al.* (1996) for the amide I band at 1650 cm^{-1}, we conclude that the effect of misalignment on the Raman polarization ratios for tryptophan markers is also small and can be neglected in comparison to the larger uncertainties described in the preceding paragraph.

SUMMARY AND DISCUSSION

We have used polarized Raman spectroscopy of *fd* fibers to assess the orientation of the W26 side chain in the pVIII subunit. The results indicate that the plane of the indole ring is nearly parallel ($0 \pm 10°$) to the virion axis and that the pseudo-2-fold axis of the indole ring forms an angle of $36 \pm 3°$ with the virion axis. These structural results, which are independent of any assumed *fd* model, are depicted in Figure 5B.

The present determination of the W26 orientation in *fd* by polarized Raman spectroscopy is based upon the key assumption that tryptophan Raman tensors determined previously for the *N*-acetyl-L-tryptophan (*N*-AcTrp) single crystal are transferable to W26. Specifically, we have assumed that Raman tensors for the normal modes $\omega3$ (1557 cm^{-1}), $\omega7$ (1357 cm^{-1}), and $\omega7'$ (1332 cm^{-1}) of *N*-AcTrp are the same as those for the corresponding modes (1560, 1364, and 1340 cm^{-1}) of W26 in subunits of the *fd* fiber. This assumption cannot be proven but is supported by the fact that the Raman frequencies and relative intensities closely parallel one another in the two structures. Raman spectra of *N*-AcTrp in both single crystals and aqueous solutions reveal that the $\omega3$, $\omega7$, and $\omega7'$ bands are largely unperturbed by the change in the molecular environment (Tsuboi *et al.*, 1996). Additionally, the depolarization ratios (ρ) measured on isotropic solutions of *N*-AcTrp and L-tryptophan are essentially identical ($\rho = 0.15 \pm 0.05$ for $\omega3$, $\rho = 0.17 \pm 0.03$ for $\omega7$, and $\rho = 0.15 \pm 0.05$ for $\omega7'$; Tsuboi *et al.*, 1996). This suggests that the corresponding Raman tensors are largely independent of covalent changes external to the indole moiety. Thus, there is considerable experimental evidence to support the assumption of transferability of the Raman tensors. The reliability of this assumption will be further tested in future work on single crystals of other tryptophan-containing compounds of known structure (Miura *et al.*, 1989).

In order to develop a more detailed molecular model of the W26 side chain conformation and indole ring orientation, it is instructive to combine the present polarized Raman results with a previous Raman determination of the side-chain torsion $\chi^{2,1}$ (C2−C3−Cβ−Cα torsion angle) (Aubrey & Thomas, 1991). On the basis of model compound studies (Miura *et al.*, 1989), it is known that the Raman marker band of tryptophan in the spectral interval 1545−1560 cm^{-1} (normal mode $\omega3$) is diagnostic of the absolute magnitude of the torsion $\chi^{2,1}$. In the case of *fd*, the Raman band is observed at 1560 cm^{-1} (Aubrey & Thomas, 1991), which indicates $|\chi^{2,1}| = 120 \pm 10°$. To resolve the ambiguity in the sign of $\chi^{2,1}$ and also to establish a compatible value for the torsion χ^1 (C3−Cβ−Cα−N) of W26, we have examined all pairs of χ^1 and $\chi^{2,1}$ torsions consistent with the Raman results and the tryptophan side-chain rotamer library of Ponder and Richards (1987). We have also imposed the criterion that the W26 orientation be energetically favorable in the context of the *fd* assembly, as judged by energy minimization (Brünger, 1992) of the most recent *fd* model of Marvin and co-workers (Marvin *et al.*, 1994; Symmons *et al.*, 1995; Protein Data Bank identification number 1IFJ). Our criteria suggest the ranges $+101° < \chi^{2,1} < +120°$ and $-84° < \chi^1 < -70°$ for side-chain torsions of W26.

On the basis of the above considerations, we propose a plausible energy-minimized model of the *fd* subunit α-helix in the vicinity of W26 (residues 22−30), as shown in Figure 6. The N terminus of the subunit α-helix is at the top in this illustration. In this model, the χ^1 and $\chi^{2,1}$ torsions of W26 are within the allowable ranges described above, viz. at −76 and +108°, respectively. The indole plane is tilted by a small angle (20°) from the virion axis, while the pseudo-2-fold axis is directed at 44° with respect to the axis. The latter two parameters differ only marginally from the experimentally determined structure which is depicted in Figure 5B.

In the course of this analysis, we observed that the pVIII subunit in the proposed 1IFJ model of Marvin and co-workers has W26 torsions $\chi^1 = -115°$ and $\chi^{2,1} = -70°$ (Symmons *et al.*, 1995). Although these torsions are not inconsistent with the indole plane orientation deduced from the polarized Raman data (Figure 5B), they violate the Miura *et al.* (1989) correlation established for $\omega3$ and are not consistent with either the library of Ponder and Richards (1987) or the indole orientation established from UVRR studies of flow-oriented *fd* (Takeuchi *et al.*, 1996; see below). Interestingly, these inconsistencies can be resolved simply by exclusion of the negative sign for $\chi^{2,1}$. (Energy minimization also indicates that the 1IFJ X-ray model can accommodate quite well a 180° flip of $\chi^{2,1}$ from −70 to +110° with an accompanying change in χ^1 from −115 to approximately −80° and modest adjustments in the peptide ϕ,ψ torsions.)

It is of further interest to compare the present results with a determination of W26 orientation in hydrodynamically oriented *fd* virions, as measured by ultraviolet resonance Raman (UVRR) spectroscopy in combination with Raman linear intensity difference (RLID) (Takeuchi *et al.*, 1996). The UVRR−RLID study has revealed that for dilute aqueous *fd* (≈1 mg/mL) the plane of the W26 indole ring is inclined by a small angle ($31 \pm 4°$) from the virion axis, while the indole pseudo-2-fold axis is directed at $38 \pm 6°$ from the virion axis. Thus, both fiber and solution determinations yield, within experimental error, the same result for the orientation of the indole pseudo-2-fold axis; they are distinguished only by a modest difference in the tilt of the indole plane with respect to the virion axis. The presently refined model (Figure 6) in fact agrees very closely with the model proposed on the basis of the UVRR−RLID study [Figure 12 of Takeuchi *et al.* (1996)]. The very small difference in indole plane tilt (∼10°) in the two models may reflect a structural difference between fibrous and solution states of *fd* or may result from inadequacies in the approximations employed in the two methods. The former explanation is consistent with the notion that subunit interactions in the filamentous virion assembly are sensitive to local solvent and salt environments (Thomas *et al.*, 1983).

In an earlier study, Clack and Gray (1992) employed UV linear dichroism spectroscopy (UVLD) to estimate the orientation of the W26 side chain in dilute solutions of *fd*. They deduced an upper limit of 43° for the tilt angle of the indole plane but did not exclude smaller values. Accordingly, the UVLD estimate does not conflict with either the polarized Raman or UVRR−RLID determinations. The disposition of the indole pseudo-2-fold axis was not determined in the UVLD study.

The model proposed in Figure 6 provides a basis for further evaluation of virion architecture in the vicinity of residue W26. Previous studies (Overman *et al.*, 1994; Overman & Thomas, 1995) show that the local environment

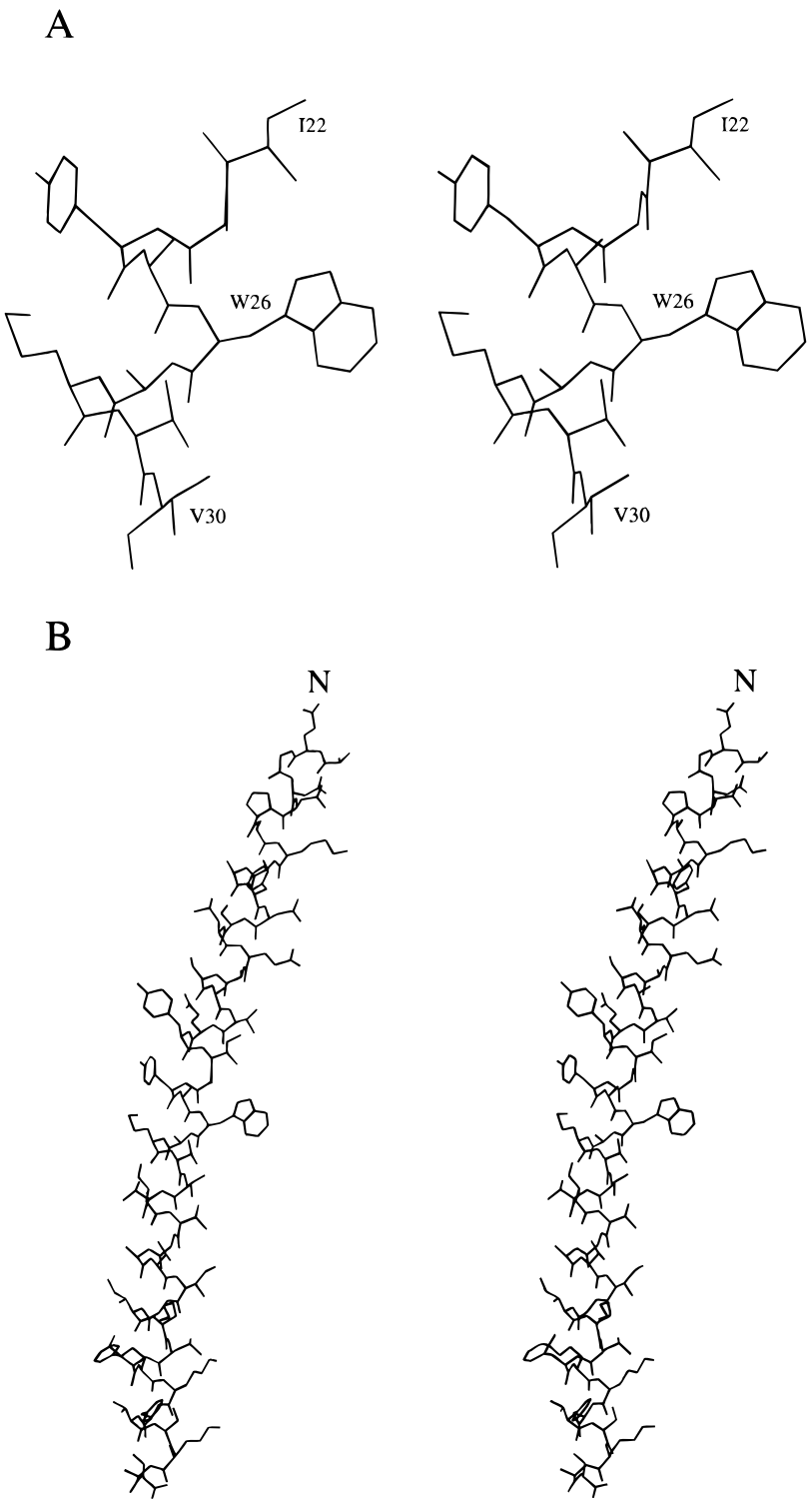

FIGURE 6: (A) Stereodiagram of an energy-minimized (Brünger, 1992) structural model proposed for the native *fd* subunit in the vicinity of the W26 side chain (residues 22−30). The model is based upon the indole ring orientation obtained from the polarized Raman results of Figure 5, the W26 side-chain torsion $\chi^{2,1}$ indicated by tryptophan normal mode ω3 (Aubrey & Thomas, 1991), the average tilt angle (16°) of the subunit α-helical axis with respect to the virion axis determined by polarized Raman microspectroscopy (Overman *et al.*, 1996), and the fiber diffraction-based symmetry of the *fd* virion (Marvin *et al.*, 1994; Symmons *et al.*, 1995; Brookhaven Data Bank identification code 1IFJ). The virion axis runs vertically. (B) Stereomodel of the full *fd* subunit, generated as in panel A. Molecular graphics were prepared on a Silicon Graphics workstation using the program MOLSCRIPT (Kraulis, 1991).

of the indole ring of W26 is sensitive to the mutation Y24 → M. Putative interactions of W26 and nearby residues, including Y24, with other side chains of neighboring subunits will be addressed in future polarized Raman and UVRR−RLID studies of *Ff* variants. A particularly interesting question is the significance of changes in W26 marker bands induced by changes in the salt concentration (Thomas *et al.*, 1983).

Finally, we note that the method developed here should be applicable to other biological macromolecular assemblies which exhibit a unique tryptophan environment, including the filamentous bacteriophage *Pf3*.

ACKNOWLEDGMENT

The program MOLSCRIPT was provided through the courtesy of Dr. Per J. Kraulis, Karolinska Institute (Kraulis, 1991). We thank Dr. Marilyn Yoder, UMKC, for assistance with molecular graphics. We also thank Dr. Hideo Takeuchi, Pharmaceutical Institute, Tohoku University, and Dr. Don A. Marvin, Department of Biochemistry, University of Cambridge, for providing access to results in advance of publication and for many helpful suggestions to improve the manuscript.

REFERENCES

Arnold, G. E., Day, L. A., & Dunker, A. K. (1992) *Biochemistry 31*, 7948−7956.
Aubrey, K., & Thomas, G. J., Jr. (1991) *Biophys. J. 60*, 1337−1349.
Benevides, J. M., Tsuboi, M., Wang, A. H.-J., & Thomas, G. J., Jr. (1993) *J. Am. Chem. Soc. 115*, 5351−5359.
Brünger, A. T. (1992) *X-PLOR*, Version 3.1, Yale University, New Haven, CT.
Choo, Y., & Klug, A. (1994) *Proc. Natl. Acad. Sci. U.S.A. 91*, 11163−11167.
Clack, B. A., & Gray, D. M. (1989) *Biopolymers 28*, 1861−1873.
Clack, B. A., & Gray, D. M. (1992) *Biopolymers 32*, 795−810.
Cross, T. A., Tsang, P., & Opella, S. J. (1983) *Biochemistry 22*, 721−726.
Day, L. A., Marzec, C. J., Reisberg, S. A., & Casadevall, A. (1988) *Annu. Rev. Biophys. Biophys. Chem. 17*, 509−539.
Denhardt, D. T., Dressler, D., & Ray, S., Eds. (1978) *The Single Stranded DNA Phages*, Cold Spring Harbor Laboratory Press, Plainview, NY.
Glucksman, M. J., Bhattacharjee, S., & Makowski, L. (1992) *J. Mol. Biol. 226*, 455−470.
Greenwood, G., Willis, A. E., & Perham, R. N. (1991) *J. Mol. Biol. 220*, 821−827.
Hemminga, M. A., Sanders, J. C., & Spruijt, R. B. (1992) *Prog. Lipid Res. 31*, 301−333.
Jamieson, A. C., Kim, S.-H., & Wells, J. A. (1994) *Biochemistry 33*, 5689−5695.
Kraulis, P. J. (1991) *J. Appl. Crystallogr. 24*, 946−950.
Makowski, L., & Caspar, D. L. D. (1981) *J. Mol. Biol. 145*, 611−617.
Marvin, D. A. (1990) *Int. J. Biol. Macromol. 12*, 125−138.
Marvin, D. A., Pigram, W. J., Wiseman, R. L., Wachtel, E. J., & Marvin, F. J. (1974) *J. Mol. Biol. 88*, 581−600.
Marvin, D. A., Hale, R. D., Nave, C., & Helmer Citterich, M. (1994) *J. Mol. Biol. 235*, 260−286.
Marzec, C. J., & Day, L. A. (1988) *Biophys. J. 53*, 425−440.
Miura, T., Takeuchi, H., & Harada, I. (1989) *J. Raman Spectrosc. 20*, 667−671.
Opella, S. J., & McDonnell, P. A. (1993) in *NMR of Proteins* (Gronenborn, A. M., & Clore, G. M., Eds.) pp 159−189, CRC Press, Boca Raton, FL.
Opella, S. J., Stewart, P. L., & Valentine, K. G. (1987) *Q. Rev. Biophys. 19*, 7−49.
Overman, S. A., & Thomas, G. J., Jr. (1995) *Biochemistry 34*, 5440−5451.
Overman, S. A., Aubrey, K. L., Vispo, N. S., Cesareni, G., & Thomas, G. J., Jr. (1994) *Biochemistry 33*, 1037−1042.
Overman, S. A., Tsuboi, M., & Thomas, G. J., Jr. (1996) *J. Mol. Biol. 259*, 331−336.
Ponder, J. W., & Richards, F. M. (1987) *J. Mol. Biol. 193*, 775−791.
Russel, M. (1994) *Science 265*, 612−614.
Scott, J. K., & Smith, G. P. (1990) *Science 249*, 386−390.
Smith, G. P. (1985) *Science 228*, 1315−1317.
Symmons, M. F., Welsh, L. C., Nave, C., Marvin, D. A., & Perham, R. N. (1995) *J. Mol. Biol. 245*, 86−91.
Takeuchi, H., Matsuno, M., Overman, S. A., & Thomas, G. J., Jr. (1996) *J. Am. Chem. Soc. 118*, 3498−3507.
Thomas, G. J., Jr., & Murphy, P. (1975) *Science 188*, 1205−1207.
Thomas, G. J., Jr., & Tsuboi, M. (1993) *Adv. Biophys. Chem. 3*, 1−70.
Thomas, G. J., Jr., Prescott, B., & Day, L. A. (1983) *J. Mol. Biol. 165*, 321−356.
Thomas, G. J., Jr., Benevides, J. M., Overman, S. A., Ueda, T., Ushizawa, K., Saitoh, M., & Tsuboi, M. (1995) *Biophys. J. 68*, 1073−1088.
Tsuboi, M., Ikeda, T., & Ueda, T. (1991) *J. Raman Spectrosc. 22*, 619−626.
Tsuboi, M., Ueda, T., Ushizawa, K., Ezaki, Y., Overman, S. A., & Thomas, G. J., Jr. (1996) *J. Mol. Struct. 379*, 43−50.
Williams, K. A., Glibowicka, M., Zuomei, L., Hong, L., Khan, A. R., Chen, Y. M. Y., Wang, J., Marvin, D. A., & Deber, C. M. (1995) *J. Mol. Biol. 252*, 6−14.

BI9527707